

TELERAG: EFFICIENT RETRIEVAL-AUGMENTED GENERATION INFERENCE WITH LOOKAHEAD RETRIEVAL

Chien-Yu Lin ^{*1} Keisuke Kamahori ^{*1} Yiyu Liu ^{*†2} Xiaoxiang Shi ^{†3} Madhav Kashyap ¹ Yile Gu ¹
 Rulin Shao ¹ Zihao Ye ¹ Kan Zhu ¹ Rohan Kadekodi ¹ Stephanie Wang ¹ Arvind Krishnamurthy ¹ Luis Ceze ¹
 Baris Kasikci ¹

ABSTRACT

Retrieval-augmented generation (RAG) extends large language models (LLMs) with external data sources to enhance factual correctness and domain coverage. Modern RAG pipelines rely on large datastores, creating a significant system challenge: achieving high throughput and low latency is difficult, especially when GPU memory is limited. To address these challenges, we propose TELERAG, an efficient inference system that reduces latency and improves throughput with minimal GPU memory requirements. The core innovation of TELERAG is *lookahead retrieval*, a prefetching mechanism that predicts required data and transfers them from CPU to GPU in parallel with LLM generation. In addition, TELERAG adopts a prefetching scheduler and a cache-aware scheduler to support efficient multi-GPU inference with minimal overhead. Evaluations show TELERAG achieves up to a $1.53\times$ average end-to-end latency reduction (single-query) and $1.83\times$ higher average throughput (batched), as well as good scalability in throughput. This confirms the practical utility of TELERAG for faster and more memory-efficient deployments of RAG applications.

1 INTRODUCTION

Retrieval-augmented generation (RAG) has emerged as a powerful technique to enhance large language models (LLMs) by integrating them with external databases (Gao et al., 2023b; Asai et al., 2024c; Lewis et al., 2020). During inference, RAG *retrieves* relevant content from external data sources, usually indexed as vector datastores, to mitigate issues such as hallucinations (Mallen et al., 2023; Ram et al., 2023; Khandelwal et al., 2019) and incorporate up-to-date or private information (Izacard et al., 2023; Min et al., 2023).

To provide accurate responses, modern RAG applications employ multiple rounds of LLM calls and retrievals for a single query (Gao et al., 2023b; Fan et al., 2024; Ilin, 2023; Gao, 2024; Databricks, 2024; Wei, 2024). As shown in Figure 1, RAG pipelines typically consist of four stages: (1) *pre-retrieval generation*: refines the initial user query to improve retrieval effectiveness. (2) *retrieval*: finds the relevant documents from datastore; (3) *post-retrieval generation*: generates a response based on the user’s query and retrieved documents; (4) *judgment*: Evaluates the output to

^{*}Equal contribution. [†]Work done during internship at UW.
¹Paul G. Allen School of Computer Science and Engineering, University of Washington, Seattle, USA ²Harvard John A. Paulson School of Engineering and Applied Sciences, Harvard University, Cambridge, MA, USA ³Shanghai Jiao Tong University, Shanghai, China. Correspondence to: Baris Kasikci <baris@cs.washington.edu>.

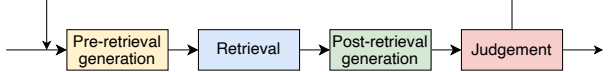


Figure 1. Typical pipeline stages of a RAG application.

determine the execution flow.

RAG datastores are typically large, as datastore size is strongly correlated with model accuracy (Min et al., 2023; Khandelwal et al., 2019; Borgeaud et al., 2022; Hardt & Sun, 2023; Shao et al.). However, a brute-force search on such a large datastore is prohibitively slow and inefficient, as most data is irrelevant to the query. This drives the adoption of solutions like the Inverted File Index (IVF) (Sivic & Zisserman, 2003), which partitions the data into clusters and restricts the search to only the most relevant ones.

While this partitioning effectively reduces the computational burden of the search, it does not solve the memory capacity challenge. To accelerate the IVF retrieval process with the GPU, one straightforward approach is to keep the entire datastore in the GPU memory (case A in Figure 2). As the size of a datastore is large (tens to thousands GB) (Quinn et al., 2025), such a setting is expensive and often commercially impractical for local and custom RAG deployments handling private or sensitive data. Even in large data centers, where user requests are often batched, this approach challenges service level objectives (SLOs) because allocating GPU memory to the datastore reduces the LLM’s key-value

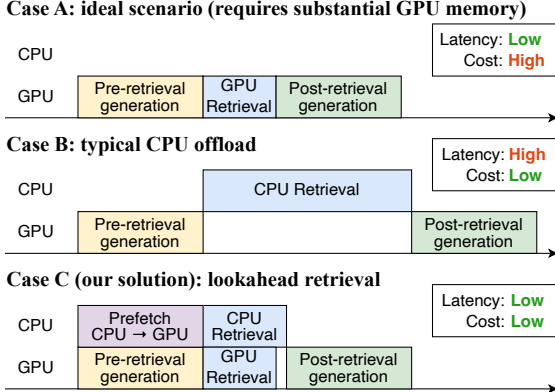


Figure 2. Illustration of TELERAG’s *lookahead retrieval* mechanism and comparison to different RAG systems. TELERAG prefetches relevant retrieval data from CPU to GPU, overlaps data transfer with the pre-retrieval stage, and accelerates retrieval with GPU–CPU cooperation.

cache (KV cache), limiting effective batch sizes (Kwon et al., 2023). An alternative approach is to load the relevant data clusters from CPU to GPU at runtime. However, because bandwidth between the CPU and GPU is typically limited, this approach suffers from high transfer latency.

As a result, modern RAG systems (Jiang et al., 2025; Shen et al., 2025) process retrieval on CPUs as they typically offer large and relatively cheap memory. However, CPUs are not as efficient as GPUs for highly parallelizable operations such as vector similarity search, and therefore using CPUs for search (case B in Figure 2) increases RAG system latency. For latency-sensitive applications such as customer chatbots (Chemmagate, 2024; Akkiraju et al., 2024; Tung, 2024), financial analysis (Malec, 2024; MyScale, 2024), and emergency medical diagnosis (Klang et al., 2024; GM & Dhar, 2024), high latency can lead to poor user experience and even critical failures. To make matters worse, any latency increase of RAG systems has compounding effects due to multiple rounds of LLM generation and retrieval.

Our proposal. In this work, we observe that there is a *substantial semantic overlap* between a user’s initial query and the query refined by an LLM during the pre-retrieval stage (see Figure 1). Since both queries represent the same core information need, their relevant IVF clusters are also likely to overlap significantly (see §3.3 for detailed analysis).

Using this insight, we propose TELERAG (§4), an efficient inference system that optimizes RAG performance by leveraging GPU retrieval acceleration while minimizing GPU memory consumption. TELERAG employs *lookahead retrieval* to proactively load relevant IVF clusters onto the GPU, hiding the CPU–GPU data transfer overhead during concurrent LLM generation. As illustrated in Figure 2, our approach aims to significantly reduce retrieval latency without exceeding GPU memory constraints. To guarantee

retrieval accuracy, TELERAG complements this prefetching with a hybrid search: any clusters missed by the lookahead are simultaneously searched on the CPU, and the results are merged. In addition to prefetching, TELERAG also utilizes on-GPU caching to further reduce redundant data transfers for frequently accessed clusters.

TELERAG also optimizes for batch and multi-GPU inference (§4.2). To mitigate increased data transfer in batched scenarios, TELERAG uses a prefetching scheduler to group similar queries, maximizing the overlap of their prefetched clusters. In multi-GPU settings, TELERAG employs a cache-aware query scheduler that routes queries to the appropriate GPU to maximize the utility of its cached clusters.

Results summary. We evaluated TELERAG using six RAG pipelines with Llama 3B/8B models (Touvron et al., 2023) on a Wikipedia datastore (AI@Meta, 2020). TELERAG demonstrates significant efficiency, enabling a datastore (61 GB) and a Llama3-8B (16 GB) LLM to run on a single RTX4090 GPU (24 GB), far exceeding CPU baseline performance. For single-query inference on an RTX4090, TELERAG achieves up to $1.53 \times$ average end-to-end latency reduction. Throughput gains increase with batching, reaching $1.83 \times$ on average (batch size 8, H100). In multi-GPU settings, its prefetching and cache-aware scheduling delivers strong scaling (e.g., on H200, $3.8 \times$ speedup on 4 GPUs, compared to the performance on 1 GPU). These results confirm TELERAG efficiently manages scalable RAG serving with low GPU memory.

In summary, we make the following key contributions:

- Analysis of the correlation of queries between the pre-retrieval generation and retrieval stages, revealing significant overlap in their corresponding IVF clusters.
- *Lookahead retrieval*, which prefetches likely IVF clusters to the GPU, and hides CPU–GPU data transfer time during pre-retrieval generation.
- TELERAG, an efficient RAG inference system that integrates *lookahead retrieval* and supports high-performance multi-GPU inference through prefetching and cache-aware scheduling, resulting in significant acceleration of RAG with minimal GPU memory usage.

2 BACKGROUND

2.1 Retrieval-Augmented Generation (RAG)

RAG is a technique that enhances the capabilities of LLMs by integrating them with information retrieval to generate more accurate and relevant text (Gao et al., 2023b; Asai et al., 2024c; Lewis et al., 2020). The core idea behind RAG is to augment the LLM with relevant information retrieved from a large corpus of documents, improving the LLM’s

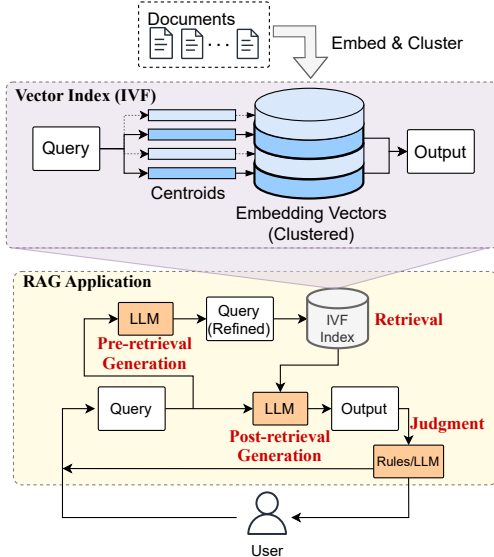


Figure 3. Overview of RAG.

ability to answer questions without hallucinations (Mallen et al., 2023; Ram et al., 2023; Khandelwal et al., 2019) and generate contents based on up-to-date or private information (Izacard et al., 2023; Min et al., 2023).

Modern RAG pipelines. In order to deliver precise and contextually appropriate responses, modern RAG models adopt a *modular* approach that employs multiple rounds of LLM calls and retrievals for a single query (Gao et al., 2023b; Fan et al., 2024; Ilin, 2023; Gao, 2024; Databricks, 2024; Wei, 2024). Typically, they have the following types of steps (shown in Figure 3): (1) **Pre-retrieval generation** decides whether retrieval is needed or polishes queries before retrieval; for example, query transformation (Ma et al., 2023; Jagerman et al., 2023; Gao et al., 2023a; Zhou et al., 2022; Ye et al., 2023; Press et al., 2023; Peng et al., 2024; Zheng et al., 2023; Liu, 2022a) reformulates the original query to make it clearer and more suitable for retrieval. (2) **Retrieval** then identifies relevant documents for the query, taking the output of pre-retrieval generation and producing the evidence for the next stage. (3) **Post-retrieval generation** uses the user’s query and the retrieved documents to produce the final response; it can also include processes like summarization (Jiang et al., 2023a; Kim et al., 2023) or reranking (Zhuang et al., 2023; Stewart & Linsdell, 2024). (4) **Judgment** component dynamically determines the execution flow (e.g., deciding whether further iteration is needed to enhance the response) using heuristics or LLMs.

2.2 Datastore, Inverted File Index (IVF), and Retrieval

Datastore. The datastore is processed by cleaning, chunking, and indexing to enable efficient retrieval. The raw data, in various formats, is first cleaned, converted to plain text, and divided into *chunks*. The chunks are then con-

verted into vector embeddings using an embedding model such as Contriever (Izacard et al., 2021). The document chunks, along with vector embeddings, are stored in a *vector database*, which enables efficient retrieval by searching for chunks based on vector similarities between the query and the chunk embeddings.

IVF-based retrieval. Many RAG deployments use the Inverted File Index (IVF) algorithm (Sivic & Zisserman, 2003) for efficient vector search. IVF partitions the vectors into *clusters* based on similarity, each represented by a *centroid*. The search is then restricted to only the few clusters most relevant to the query, avoiding searching the entire datastore.

With clustering, an IVF search is a two-step process: (1) **Cluster probing**: The query is compared only to the cluster centroids to quickly identify the few most relevant clusters. (2) **Searching**: The system then performs a detailed search only within that small set of selected clusters and returns the final top-*k* best-matching items.

A parameter called *nprobe* (Douze et al., 2024) controls the number of clusters to check in the first step. A larger *nprobe* increases accuracy at the cost of higher latency, as more data must be searched. Appendix A provides a formal description of IVF.

Latency of retrieval. Since the search process is highly parallelizable among each cluster and each vector, this search algorithm can be highly accelerated by GPUs. Furthermore, open-source libraries offer efficient GPU implementations (Johnson et al., 2019; Rapidsai, 2022). However, the vector database in modern RAG deployments can reach tens to thousands of GB (Quinn et al., 2025; Sella, 2024) as a result of the positive correlation of datastore size with accuracy (Min et al., 2023; Khandelwal et al., 2019; Borgeaud et al., 2022; Hardt & Sun, 2023; Shao et al.). The large vector databases increase the latency of RAG pipelines significantly in both local setups and data centers.

Local setups typically consist of personal workstations or laptops with a single consumer-grade GPU (e.g., RTX4090 has 24 GB of memory), where latency is critical. Data center environments, on the other hand, care about both latency and throughput since they handle numerous simultaneous user queries. In both scenarios, GPU memory capacity becomes a performance limitation when working with vector databases. Consumer GPUs in personal setups lack sufficient memory to accommodate large vector databases, whereas data-center GPUs must sacrifice KV cache space (reducing throughput) to accommodate them (Kwon et al., 2023). Consequently, vector databases are commonly stored in the CPU memory instead. Unfortunately, this approach increases retrieval latency whether IVF search operations are performed on the CPU or data must be transferred between CPU and GPU (as explored in §3).

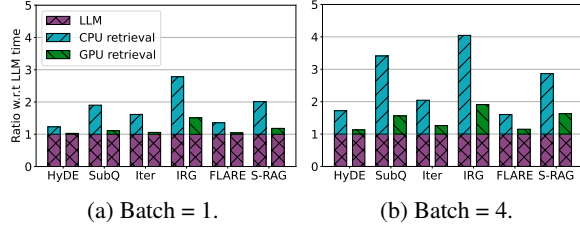


Figure 4. Latency breakdown of six RAG pipelines on NQ dataset (Kwiatkowski et al., 2019) with one H100 GPU.

3 ANALYZING RAG LATENCY

In this section, we analyze the system challenges in state-of-the-art RAG applications. We constructed a 61 GB vector index with the Faiss library (Douze et al., 2024), and set the IVF clusters to 4096 following common practice (Asai et al., 2023). Our analysis is conducted on an RTX 4090 (24 GB) and H100 (80 GB) using Llama-3-8B (AI@Meta, 2024). Further setup details are in §5.2.

3.1 End-to-end Latency of RAG Pipelines

We first analyze the end-to-end latency of six RAG pipelines (§5.1) by comparing two scenarios: (1) LLM on GPU with retrieval on CPU (low GPU memory), and (2) both LLM and the vector index on GPU (low latency).

We set the `nprobe` to 256, a commonly used setting under this index’s configuration (see §5.2 for details). As shown in Figure 4 (using randomly sampled 1024 NQ queries (Kwiatkowski et al., 2019)), the CPU-based retrieval phase is a major bottleneck, consuming 41.1% and 60.5% of total latency for batch sizes 1 and 4, respectively. In contrast, GPU-accelerated retrieval accounts for only 10.5% and 28.3% of the latency, respectively. On average, GPU retrieval is $5.96 \times$ (batch size 1) and $3.87 \times$ (batch size 4) faster than its CPU counterpart, reducing overall end-to-end latency by $1.5 \times$ and $1.8 \times$. Thus, accelerating GPU-based retrieval is crucial for reducing end-to-end latency.

However, GPU acceleration has a significant memory cost. For instance, in our setting, with a 61 GB index and a 16 GB Llama-3-8B model, GPU retrieval requires 77 GB of GPU memory, far exceeding the 24 GB of a common RTX 4090. This makes GPU-accelerated retrieval often unfeasible on lower-end GPUs or with large datastores.

Even on large GPUs (e.g., H100), storing the full index in memory limits serving throughput. High-throughput batched inference is bottlenecked by the LLM’s KV cache capacity (Kwon et al., 2023). The index’s large memory footprint reduces the available memory for this KV cache, thereby limiting the effective batch size. This memory contention is exacerbated by RAG’s typically long contexts (Jin et al., 2024a; Lu et al., 2024; Yao et al., 2024) and the growing size of models and indexes (Min et al., 2023;

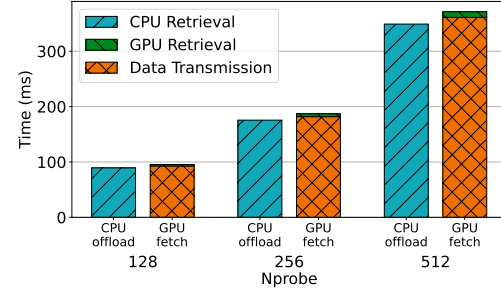


Figure 5. Latency breakdown of CPU-offload and runtime-fetch GPU retrieval, averaged over 512 random NQ queries.

Dataset	HyDE	SubQ	Iter	IRG	FLARE	S-RAG
NQ	73.1%	63.2%	91.5%	83.8%	79.1%	100.0%
HotpotQA	75.3%	62.5%	89.6%	89.4%	80.2%	100.0%
TriviaQA	73.1%	61.6%	86.2%	86.1%	81.7%	100.0%

Table 1. IVF cluster overlapping rate between the input and output of the pre-retrieval generation. Since Self-RAG does not incorporate query transform, its coverage is always 100%.

Khandelwal et al., 2019; Borgeaud et al., 2022; Hardt & Sun, 2023; Quinn et al., 2025), necessitating offloading.

Therefore, in the rest of this section, we try to answer the following question: *Is it possible to achieve the latency of GPU-based retrieval while using much less GPU memory?*

3.2 GPU-accelerated Retrieval with Runtime Transfer

A straightforward approach to enable GPU retrieval with limited GPU memory is to fetch the necessary data from CPU to GPU on demand at runtime, leveraging the IVF index to narrow the search space. While this enables fast GPU search, the data transfer itself becomes the new bottleneck.

Figure 5 compares the latency of the runtime fetching system against CPU retrieval on an RTX 4090 GPU with three different `nprobe` values that determine the amount of data fetched. Overall, fetch time dominates latency due to the limited CPU–GPU PCIe bandwidth (32 GB/s). Although the GPU search is substantially faster, the fetch overhead results in a higher end-to-end latency ($\sim 3\%$ slower on average). Thus, to achieve a meaningful speedup with this approach, the data-fetching latency must be effectively hidden.

To hide data-fetch costs, CPU-to-GPU transfers must occur before the retrieval stage, which requires predicting which data will be accessed. Fortunately, modern RAG pipelines offer a valuable hint: the query from the previous step.

3.3 Overlapping of IVF Clusters

While the exact data to be retrieved is only known after the pre-retrieval generation is done, we observe that there are high similarities of the IVF clusters assignments between the queries at different stages.

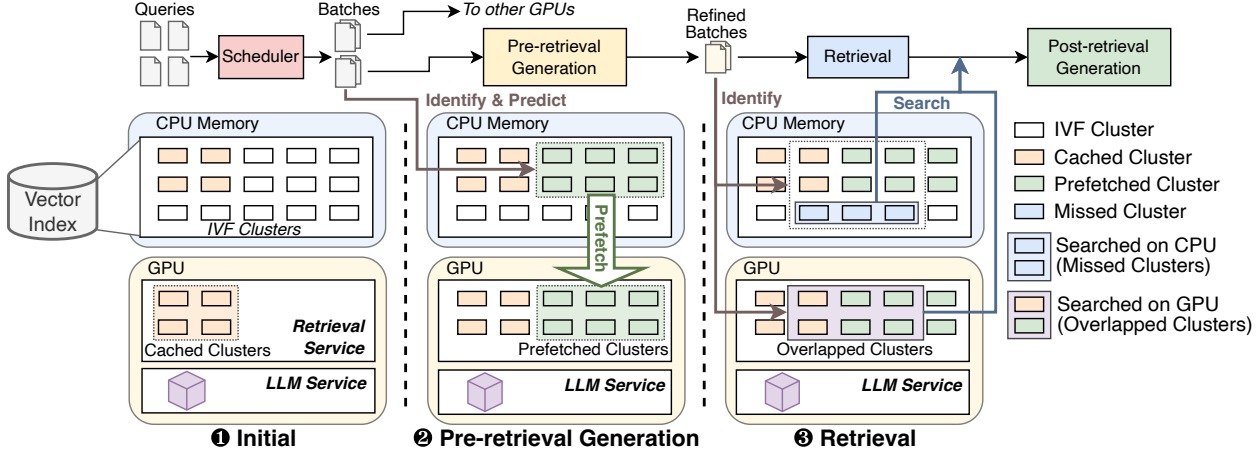


Figure 6. The overview of TELERAG system. When queries arrive, some clusters are already cached on the GPU from previous requests. These queries are grouped into micro-batches based on semantic similarity. For each micro-batch, TELERAG prefetches the required clusters using *lookahead retrieval* in parallel with the pre-retrieval generation. During retrieval, TELERAG performs a hybrid search: the GPU processes cache hits directly from GPU memory, while the CPU handles cache misses. The retrieved documents are then passed to the post-retrieval generation stage.

Similarity of queries at different stages. During RAG pre-retrieval stages (e.g., query transformation (Gao et al., 2023a; Zheng et al., 2023; Peng et al., 2023; Asai et al., 2024a)), an LLM refines an initial user query q_{in} into a transformed query q_{out} for the actual retrieval. While this process often rewrites or simplifies the query, it intuitively preserves its core semantic content. Consequently, the embedding vectors of q_{in} and q_{out} are likely to be similar, suggesting their target IVF clusters will significantly overlap. Therefore, q_{in} can serve as a valuable hint for predicting q_{out} .

Prediction coverage. To verify this hypothesis, we evaluated the average cluster coverage (predicted vs. actual) in three popular QA datasets (NQ (Kwiatkowski et al., 2019), HotpotQA (Yang et al., 2018), and TriviaQA (Joshi et al., 2017)) and six RAG pipelines. As Table 1 shows, when prefetching 256 clusters, the overlap is consistently high. For instance, even the lowest reported coverage (for SubQ) remains above 61.6%.

Opportunity. This data shows an opportunity to predict required clusters, hiding data transfer overhead during LLM generation. In this paper, we aim to leverage this observation to accelerate the inference latency for RAG.

4 DESIGN OF TELERAG

Driven by the need for high-performance but memory-efficient RAG inference, we propose TELERAG, an end-to-end system that accelerates retrieval through its core **lookahead retrieval mechanism**, which accelerates the retrieval process with a GPU but only requires a small fraction of the datastore on the GPU memory. Alongside this technique, TELERAG further designs optimizations on caching,

prefetching amount, and scheduling algorithms for batching and multi-GPU scenarios, forming a complete system for both local and cloud usages.

This section details the lookahead retrieval mechanism (§4.1), and then describes how TELERAG extends it with batching and multi-GPU support (§4.2), followed by other system-level optimizations (§4.3). Appendix C provides implementation details.

4.1 Lookahead Retrieval Mechanism

The core mechanism of TELERAG, lookahead retrieval, is inspired by the observation in §3.3 that queries across different RAG stages are highly correlated and therefore select overlapping IVF clusters. Building on this insight, lookahead retrieval predicts and prefetches likely-needed clusters to the GPU during LLM generation, overlapping data transfer with computation. During retrieval, TELERAG leverages lookahead retrieval to coordinate the CPU and GPU so that prefetched data are processed on the GPU, while the CPU concurrently handles any missed clusters. This cooperative execution forms the foundation of TELERAG’s low-latency, memory-efficient design.

Figure 6 shows the overview of TELERAG with lookahead retrieval. Let q_{in} denote the query input to the pre-retrieval stage and q_{out} denote the output passed to the retrieval stage. The IVF clusters selected by q_{in} and q_{out} are highlighted with a green background (C_{in}) and a purple background (C_{out}), respectively. Due to the semantic similarity between q_{in} and q_{out} , there is substantial overlap between C_{in} and C_{out} .

Guided by this correlation, lookahead retrieval operates in the following steps:

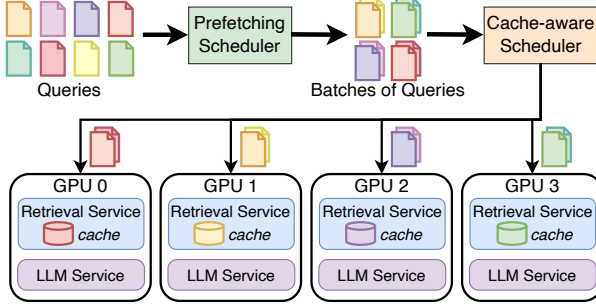


Figure 7. Overview of TELERAG’s multi-GPU system design. The prefetching scheduler clusters semantically similar queries into micro-batches, while the cache-aware scheduler assigns these batches to GPUs based on cache locality.

1. **Predict & prefetch:** During LLM generation, prefetch IVF clusters likely to be used in retrieval to GPU memory, identified by their distance to q_{in} . This transfer is performed asynchronously via GPU DMA, overlapping with ongoing LLM computation.
2. **GPU similarity search:** Once q_{out} is available, the GPU efficiently searches the predicted clusters ($C_{overlap}$) already resident in GPU memory.
3. **CPU similarity search:** Concurrently, the CPU performs similarity search over the remaining clusters (C_{miss}) that were not prefetched.
4. **Merge:** The search results from GPU and CPU are merged on GPU. The retrieval documents are fed to LLM for post-retrieval generation on GPU.

In summary, lookahead retrieval enables TELERAG to accelerate retrieval by overlapping data prefetching with LLM generation and distributing the similarity search between GPU and CPU. This design significantly reduces CPU computation and data transfer latency, forming the backbone of TELERAG’s efficiency.

Prefetching amount. Prefetching more clusters improves hit rate and retrieval speed, but also increases CPU–GPU transfer time. If this transfer exceeds the pre-retrieval generation window, the overlap advantage is lost and may add latency, though slight overruns are acceptable if retrieval savings are substantial. Through analytical modeling and empirical profiling on modern hardware, we found *prefetching up to the pre-retrieval LLM generation time* (t_{LLM}) achieves the optimal balance between latency reduction and transfer overhead. A detailed derivation of this result is provided in Appendix B. Since t_{LLM} varies per query, for a given pipeline and hardware bandwidth B_{link} , we estimate its average (\bar{t}_{LLM}) on a calibration set and set the prefetching amount to $B_{link} \times \bar{t}_{LLM}$.

4.2 Batching and Multi-GPU System

While §4.1 describes lookahead retrieval on a single query and single GPU basis, we now demonstrate how TELERAG extends this mechanism to support batches and multi-GPU inference. The system’s multi-GPU architecture is illustrated in Figure 7.

Batching design. For batched scenarios, a challenge for lookahead retrieval is that each query requires a different set of IVF clusters. In our design, we apply the fixed total prefetching budget as described in §4.1, and distribute it equally among all queries in the batch. Although the per-query hit rate drops as the batch size grows, this strategy provides balanced retrieval acceleration for each query.

Multi-GPU support. In multi-GPU scenarios that serve a large number of RAG queries, TELERAG divides a global batch of queries into micro-batches and assigns them to each available GPU. Each GPU then independently processes the full RAG pipeline for its assigned micro-batches.

Scheduling optimization for prefetching. To compensate for the reduced hit rate in larger batches, we introduce a *prefetching scheduler* (see Figure 7). It operates by performing a greedy search on the global batch, grouping queries by the lowest L2 distance. While this scheduling adds latency, the greedy search is highly efficient on GPUs, incurring negligible overhead. Our profiling shows that for batch sizes up to 256, the search latency is less than 0.1 s, which is minimal compared to the end-to-end batch latency.

Cache design. To improve performance, TELERAG implements a dynamic caching strategy for data clusters. Instead of discarding all clusters after a request is served, it retains the most frequently accessed ones in GPU memory. This allows subsequent requests to reuse these cached clusters, boosting the cache hit rate and prefetching efficiency.

Cache-aware scheduling. To further exploit the benefits of caching, we design a cache-aware scheduler (Figure 7) that assigns micro-batches to GPUs based on cache locality. The scheduler employs a greedy strategy: it first selects the micro-batch with the greatest overlap across all GPU caches and assigns it to the best-matching GPU. It then iteratively schedules the remaining micro-batches in descending order of overlap with each GPU’s cached clusters. Although this scheduling introduces minor overhead, the performance gains from improved cache locality outweigh the cost (§5.4).

4.3 System Optimizations

GPU sorting. TELERAG accelerates the final sorting stage of IVF search by leveraging the GPU. To achieve this, TELERAG transfers the scalar distance values of C_{miss} from the CPU to the GPU. Unlike transferring full vector data, this operation is lightweight and incurs negligible overhead.

Setup	Desktop	Server1	Server2
CPU	Threadripper 5975	EPYC 9554	EPYC 9534
CPU mem. size	512 GB	1.5 TB	1.5 TB
GPU	RTX4090	H100	8×H200
GPU mem. size	24 GB	80 GB	140 GB
CPU-GPU Bus Bandwidth	PCIe 4 32 GB/s	PCIe 5 64 GB/s	PCIe 5 64 GB/s

Table 2. Hardware specifications for our setups.

The GPU then performs a global sort over the combined distances of C_{miss} and C_{overlap} .

Prefetching target. TELERAG prefetches a fixed byte budget (b_p), rather than a cluster count, to ensure predictable transfer times given highly uneven cluster sizes. The system fills this budget by adding whole clusters sequentially based on query proximity. If the next closest cluster exceeds the remaining budget, it is skipped entirely, ensuring a clean GPU/CPU processing split.

Prefetching for multi-round. For multi-round RAG involving the same input query, the system performs a full prefetch (up to the budget) only in the first round, leveraging high cluster similarity across rounds. In subsequent rounds, it incrementally fetches only the additional required clusters that were not loaded previously, optimizing data transfer while respecting the memory budget.

5 EVALUATION

We conducted extensive experiments to evaluate the effectiveness of TELERAG. In this section, we describe the necessary details on evaluation setups, present experimental results, and provide in-depth analysis and discussions.

5.1 Evaluation Datasets and RAG Models

Datastore. We built a datastore based on the wiki_dpr dataset (Karpukhin et al., 2020), a popular dataset that contains 2.1 billion tokens from Wikipedia. Following previous works (Asai et al., 2023; Karpukhin et al., 2020; Min et al., 2023), we chunked the passages by every 100 tokens, and used Contriever (Izacard et al., 2021) to generate an embedding for each chunk. The embeddings have a hidden dimension of 768. The index size is 61 GB and we clustered the embeddings into 4096 IVF clusters. See Appendix D for detailed configurations of the index.

LLMs. We evaluated TELERAG on the Llama model family (Touvron et al., 2023) in two different sizes (Llama-3.2-3B, Llama-3-8B) to represent different use cases.

RAG pipelines. We evaluated TELERAG with six popular RAG pipelines, as depicted in Figure 8. Note that even in pipelines lacking a pre-retrieval stage, the post-retrieval generation serves a similar function for the next retrieval

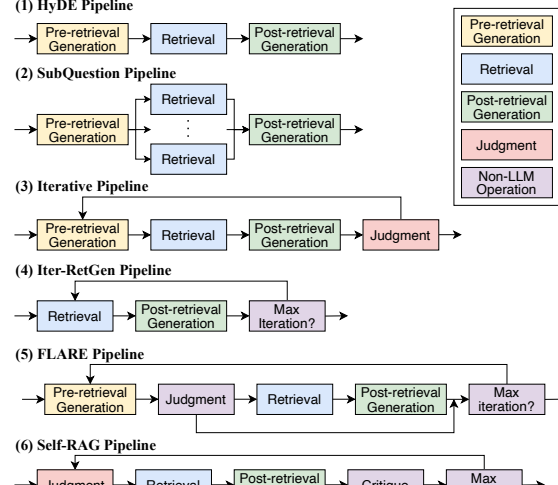


Figure 8. Overview of six RAG pipelines that we evaluate.

iteration. Below are brief descriptions of these pipelines.

1. **HyDE** (Gao et al., 2023a) prompts LLM to generate a hypothetical paragraph and perform retrieval based on the embedding of the generated paragraph.
2. **SubQuestion (SubQ)** (Liu, 2022c) prompts LLM to generate multiple sub-questions and performs retrievals for each generated sub-question.
3. **Iterative (Iter)** (Liu, 2022b) prompts LLM to generate narrower questions first and iteratively refine them based on previous answers. At the end of each iteration, it prompts LLM to judge if the answer is good enough.
4. **Iter-RetGen (IRG)** (Shao et al., 2023) iteratively does retrieval and LLM generation for 3 iterations.
5. **FLARE** (Jiang et al., 2023c) iteratively issues retrievals based on the confidence (probability score) of predicted tokens for the upcoming sentence.
6. **Self-RAG (S-RAG)** (Asai et al., 2023) uses the LLM to judge for retrieval, generate responses, and self-critique on the responses. We use the fine-tuned model based on Llama2-7B from their official repository (Asai et al., 2024b) for trace generation.

Evaluation datasets. We use three commonly used question-answering datasets, NQ (Kwiatkowski et al., 2019), HotpotQA (Yang et al., 2018), and TriviaQA (Joshi et al., 2017). For each dataset, we randomly sampled 1024 queries and reported the average. When cache is enabled, to ensure stable results and avoid an initial low hit rate from a cold start, we use 512 queries for warming up the cache and another different 512 queries for evaluation.

5.2 Experiment Setups

Hardware setups. We evaluated TELERAG on three hardware environments, Desktop, Server1 and Server2,

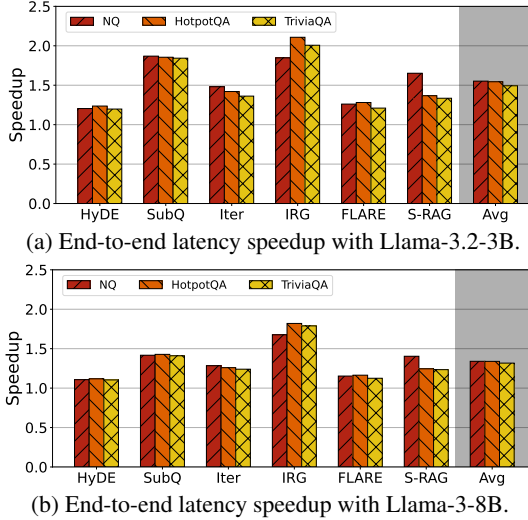


Figure 9. End-to-end latency speedup of TELERAG and baseline on six RAG pipelines and three datasets, with RTX4090 GPU.

which are equipped to represent the settings for the desktop and data center use cases. The Desktop has the RTX4090, and we use the 3B and 8B models, which are the commonly used model sizes for RAG applications (Asai et al., 2023; 2024a). For Server1 (H100) and Server2 (H200), we use the 8B model. We use Server1 for single GPU evaluation and Server2 (8 GPUs) for multi-GPU evaluation. Table 2 summarizes the hardware configurations.

Nprobe and top- k . A common heuristic for the IVF index is to set nprobe to $4\sqrt{N_c}$ (Zilliz, 2020). Given our index size of $N_c = 4096$, we use nprobe = 256 ($= 4\sqrt{4096}$) by default, unless otherwise specified. For retrieval, we use top- k = 3 for the number of documents to return, unless otherwise specified.

RAG pipeline implementation. We implemented the RAG pipelines with the FlashRAG framework (Jin et al., 2024b). For IRG, FLARE, and S-RAG, we used the framework’s default implementations. For the other pipelines, we reimplemented them using FlashRAG’s APIs.

Benchmark methodology. We follow a benchmarking methodology from SGLang (Zheng et al., 2024) and use GPT-3.5-Turbo (OpenAI) to run through each pipeline and record the input and output text of each step. During latency evaluation, we set the LLM’s output length based on the recorded text. This way, we ensure a fair latency comparison across different LLM models.

Baseline systems. To evaluate the latency of each pipeline, we constructed a clean execution flow in Python that only contains LLM generation, datastore retrieval, and other necessary logical operations to fulfill each pipeline. For LLM generation, we used SGLang (Zheng et al., 2024), which is a state-of-the-art LLM inference engine. For retrieval, we used a popular retrieval library, Faiss (Douze et al., 2024),

as the CPU-offloaded baseline.

Prefetching budget setups. Based on the methodology we described in §4.1, we profiled each RAG pipeline with 64 random samples from NQ (Kwiatkowski et al., 2019) and derived the prefetching budget of each pipeline. Since H100 and H200 have the same CPU–GPU bandwidth, we set the same prefetch budget for Server1 and Server2.

Max GPU memory for retrieval. We set a maximum GPU memory limit for prefetching in each configuration. For Server1 and Server2, we allocated 12 GB and 24 GB, respectively. For Desktop, we allocated up to 10 GB and 3.75 GB for the 3B and 8B models, respectively.

Cache Setup. The memory allocated for retrieval is shared between prefetching and caching. In our evaluation, we set the cache proportion to 50% (*i.e.*, cache can use at most half of this memory). Since the benefit of caching is negligible on a single GPU (demonstrated in the ablation study), we enabled it only for the multi-GPU experiments on Server2.

5.3 Evaluation Results

Single-query latency on RTX4090. We evaluated the end-to-end RAG latency for single query on Desktop equipped with a RTX4090, representing the typical local scenario. Figure 9 shows the latency reduction of TELERAG across three datasets and two LLMs (Llama-3.2-3B and Llama-3-8B). As Figure 9 shows, TELERAG consistently outperforms the CPU-offload baseline across all evaluated configurations. With Llama-3.2-3B, TELERAG achieves average speedups of $1.55\times$, $1.54\times$, and $1.49\times$ on NQ, HotpotQA, and TriviaQA, respectively.

Among the test pipelines, the best speedup of $2.11\times$ is achieved in the Iter-RetGen pipeline on HotpotQA, because this pipeline involves frequent retrieval operations and generally short LLM outputs, which enhances the relative impact of retrieval acceleration. Another notable improvement is in the SubQuestion pipeline, where TELERAG achieves approximately $1.85\times$ speedup across all datasets. This pipeline uses LLM-generated sub-questions and performs batched retrievals of 3 to 4 queries in its retrieval stage. CPU-based retrieval suffers from limited parallelism in such scenarios, but TELERAG efficiently utilizes GPU parallelism, significantly enhancing performance.

When deploying Llama-3-8B, speedups with TELERAG slightly decrease compared to Llama-3.2-3B, primarily due to increased LLM latency and reduced available memory for prefetching. Still, TELERAG achieves approximately $1.3\times$ speedup across datasets, with a peak improvement of $1.82\times$ for Iter-RetGen pipeline on HotpotQA. Achieving these results with only 3.75 GB of remaining GPU memory (after accounting for Llama-3-8B (16 GB), the embedding model (1 GB), and other miscellaneous tensors) highlights TEL-

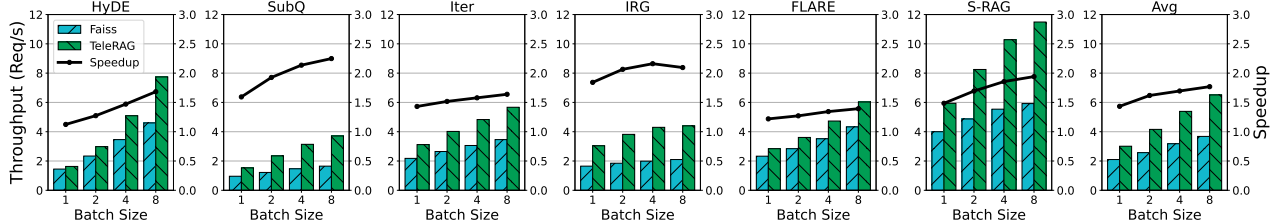


Figure 10. End-to-end throughput of TELERAG and the CPU-offload baseline across six RAG pipelines on the NQ dataset using Llama-3-8B, evaluated at different batch sizes on a H100 GPU.

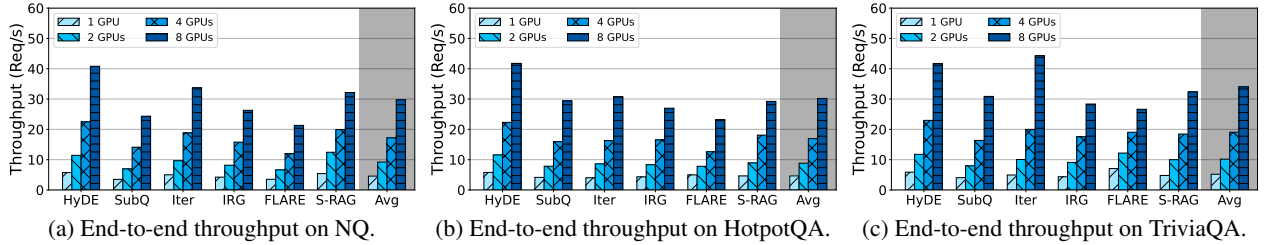


Figure 11. Throughput scaling of TELERAG across multiple H200 GPUs. Global batch fixed at 128; micro-batch fixed at 4.

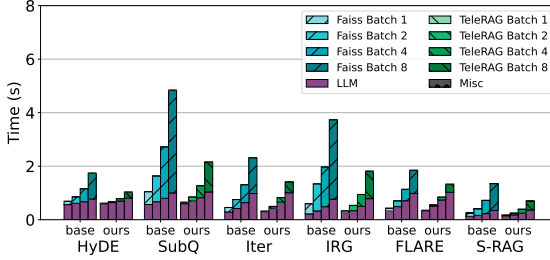


Figure 12. Latency breakdown for Llama-3-8B on NQ with a H100 GPU in different batch sizes. n_{probe} is 256.

Pipeline	H100 (Llm3-8B)		4090 (Llm3-3B)	
	Budget	Hit Rate	Budget	Hit Rate
HyDE	9 GB	91.95%	7 GB	87.42%
SubQ	8 GB	79.04%	7 GB	76.38%
Iter	5 GB	95.51%	3 GB	84.59%
IRG	4 GB	59.52%	2.5 GB	50.34%
FLARE	6 GB	79.35%	3 GB	56.67%
S-RAG	3 GB	71.29%	1.25 GB	29.96%

Table 3. The prefetch budget and corresponding averaged cluster hit rate for each pipeline and hardware setup on NQ dataset. The target retrieval n_{probe} is 256.

ERAG’s robust capability in accelerating RAG inference even under tight GPU memory constraints.

Multi-query throughput on H100. To illustrate TELERAG’s performance in batched inference, we evaluated the end-to-end throughput on Server1 (H100) using batch sizes 1, 2, 4, and 8. The results of six RAG pipelines with Llama-3-8B are presented in Figure 10.

As shown in Figure 10, TELERAG consistently outperforms the Faiss baseline across all pipelines and batch sizes. At

batch size 1 and running with Llama-3-8B (equivalent to the single-query setting), TELERAG delivers a throughput increase of $1.1\times$ to $2.2\times$, with an average of $1.45\times$. As the batch size increases, the performance gains of TELERAG continually grow. The Faiss baseline demonstrates near-linear scalability up to a batch size of 4, but reaches a noticeable plateau at a batch size of 8, indicating that the CPU baseline’s capacity to handle a high volume of simultaneous queries is limited. In contrast, TELERAG continues to scale nearly linearly through the largest batch evaluated, reaching $1.4\text{--}2.2\times$ higher throughput and an average throughput increase of $1.83\times$ at batch 8. The biggest throughput gain is achieved for SubQuestion, up to $2.2\times$ at batch 8. This is again due to their higher demands on the retrieval, leaving higher optimization space for TELERAG.

Multi-GPU throughput. We evaluate TELERAG’s scalability on Server2 (H200), a multi-GPU system. Figure 11 reports throughput for a global batch size of 128 with a micro-batch size of 4 across 1–8 GPUs, with both the prefetching and cache schedulers enabled. TELERAG scales well with the number of GPUs: on NQ, compared to single GPU case, the average speedups are $2.0\times$, $3.8\times$, and $6.5\times$ on 2, 4, and 8 GPUs, respectively. The mild sub-linear scaling at higher GPU counts is attributed to execution time variance across micro-batches—specifically, a long tail of higher-latency batches that create load imbalance. These results still demonstrate that the lookahead retrieval technique in TELERAG can scale effectively.

5.4 Analysis and Sensitivity Study

Latency breakdown. We further show the latency breakdown of running RAG pipelines with Llama-3-8B on a single H100 GPU in different batch sizes in Figure 12. From

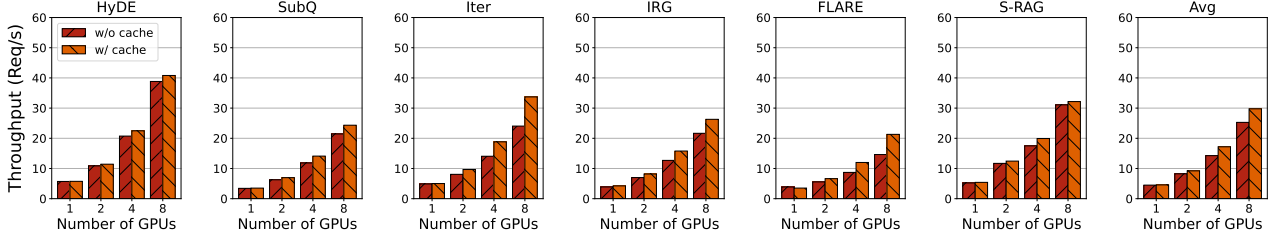


Figure 13. Throughput of TELERAG on the NQ dataset with different numbers of H200 GPUs (with and without cache).

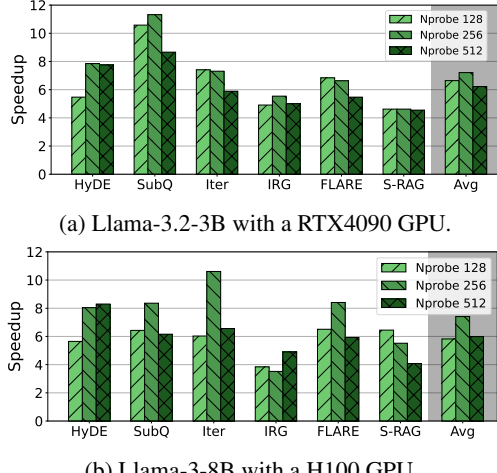


Figure 14. Single-query retrieval speedup on NQ with different nprobe values.

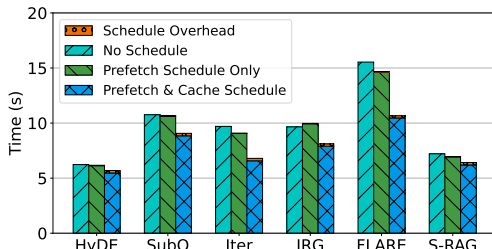


Figure 15. Comparison of end-to-end latency for prefetching and cache-aware schedulers on 4 H200 GPUs. The overhead bars of prefetch schedule only are too short to be visible.

Figure 12, we can observe that LLM latency grows sub-linearly with larger batch sizes. However, the latency for Faiss retrieval on CPU grows linearly with the batch size, dominating the overall latency when batch size is large. These results echo our findings in Figure 10, and show limited scalability of CPU retrieval in serving scenarios. In contrast, TELERAG significantly accelerates across all batch sizes and achieves a higher speedup from $1.4\times$ to $1.8\times$ when the batch size increases from 1 to 8.

Prefetch budgets and cluster hit rates. Table 3 shows the prefetch budgets we set with the profile-guided approach on RTX4090 and H100 for NQ. It also presents the average cluster hit rate achieved with this prefetch budget. From the table, we can see that it generally achieves a high cluster

hit rate ($>50\%$) when TELERAG has a large prefetching budget. For cases where the budget is less than 2 GB, we observe a relatively lower hit rate ($<50\%$), limiting the benefits of reducing the CPU’s search workloads. However, as observed from Figure 9, TELERAG achieves from $1.2\times$ to $1.6\times$ end-to-end speedups for these pipelines, thanks to the combined benefit of reducing CPU workload and utilizing the GPU to perform sorting on similarity distances.

Retrieval speedups across nprobe. Figure 14 shows the retrieval latency reduction on NQ. We observe consistent speedups for all nprobe values. The greatest speedups are achieved at nprobe 256, with average speedups of $7.21\times$ and $7.41\times$ on RTX4090 and H100, respectively. As a larger nprobe value is used, the retrieval performance of TELERAG becomes constrained by missed clusters on the CPU, given our fixed prefetch budget across varying nprobe values. However, RAG inference with higher nprobe will result in longer latency spent on the retrieval and hence, TELERAG still has a significant latency improvement against the CPU retrieval baseline.

Ablation on cache. Figure 13 illustrates the throughput improvements enabled by caching on the NQ dataset. On average, caching boosts throughput of 2%, 12%, 21%, and 18% with 1, 2, 4, and 8 GPUs, respectively. The benefit on a single GPU is marginal because only a small cache space is used, and the limited cache capacity struggles to accommodate diverse requests. However, as the number of GPUs and overall cache space increases, the cache-aware scheduler effectively assigns micro-batches to the appropriate GPUs to maximize cache overlap, thereby improving prefetching hit rates and yielding significant throughput gains.

Analysis on scheduling overhead. Figure 15 analyzes the benefits and overheads of the prefetching and cache-aware schedulers. It reports the end-to-end latency for a global batch of 128 queries with a mini-batch size of 4 on 4 H200 GPUs, comparing configurations that enable both schedulers, only the prefetching scheduler, or neither. As shown in Figure 15, the prefetching scheduler incurs only a minimal overhead of approximately 37 ms (thus almost invisible in the figure), while the cache-aware scheduler adds a modest overhead of about 220 ms. Overall, both schedulers effectively reduce end-to-end latency in most cases, with minimal additional cost.

6 RELATED WORK

Systems for RAG. Prior works have accelerated RAG by caching the LLM’s KV cache from retrieved documents (Jin et al., 2024a; Lu et al., 2024; Yao et al., 2024). However, these approaches primarily reduce prefill latency, failing to address the retrieval and decode latencies which often dominate. Other techniques, like speculative retrieval (Zhang et al., 2024b) or fine-grained pipelining (Jiang et al., 2024), target different RAG paradigms (e.g., per-token retrieval) and do not apply to the widely-used modular pipelines discussed in §2.1. Unlike these approaches, TELERAG is the first to tackle the fundamental system challenges of long retrieval latency and large memory requirements for modular RAG with large-scale datastores.

Systems for compound LLM applications. Apart from RAG, there is a growing interest in compound or agentic LLM applications, where multiple LLM calls and other applications are combined to serve complex functionalities (Zaharia et al., 2024; Berger & Zorn, 2024; Wang et al., 2024). AI Metropolis (Xie et al., 2024) accelerates LLM-based multi-agent simulations with out-of-order execution. RAG is a specific type of application in this broader direction, and we propose systems techniques to optimize its execution latency, focusing on the characteristics of retrieval workload.

Vector Index. A separate line of work focuses on optimizing the vector index itself. This includes hardware-specific acceleration (GPU (Johnson et al., 2019), FPGA (Jiang et al., 2023b)) and hybrid memory-disk systems to scale beyond RAM (DiskANN (Jayaram Subramanya et al., 2019), SPANN (Chen et al., 2021)). More recent systems scale graph-based indexes beyond GPU memory (Khan et al., 2024; Zhang et al., 2024a). These methods often require significant algorithm modifications or remain bottlenecked by CPU–GPU bandwidth. TELERAG is complementary, optimizing at the system-level by hiding transfer latency within the RAG application’s context, without altering the underlying IVF algorithm.

7 CONCLUSION

In this paper, we introduced TELERAG, an inference system that improves RAG pipeline latency and throughput while imposing minimal GPU memory requirements. TELERAG achieves significant acceleration by employing *lookahead retrieval*, which hides CPU–GPU data transfer latency by overlapping it with pre-retrieval generation, and by supporting efficient multi-GPU inference through specialized scheduling. Our evaluation shows that TELERAG significantly improves performance compared to existing state-of-the-art solutions and scales effectively with increased hardware resources.

REFERENCES

AI@Meta. Dataset card for “wiki_dpr”. https://huggingface.co/datasets/facebook/wiki_dpr, 2020.

AI@Meta. Llama 3 model card. https://github.com/meta-llama/llama3/blob/main/MODEL_CARD.md, 2024.

Akkiraju, R., Xu, A., Bora, D., Yu, T., An, L., Seth, V., Shukla, A., Gundecha, P., Mehta, H., Jha, A., et al. Facts about building retrieval augmented generation-based chatbots. *arXiv preprint arXiv:2407.07858*, 2024.

Ansel, J., Yang, E., He, H., Gimelshein, N., Jain, A., Voznesensky, M., Bao, B., Bell, P., Berard, D., Burovski, E., Chauhan, G., Chourdia, A., Constable, W., Desmaison, A., DeVito, Z., Ellison, E., Feng, W., Gong, J., Gschwind, M., Hirsh, B., Huang, S., Kalambarkar, K., Kirsch, L., Lazos, M., Lezcano, M., Liang, Y., Liang, J., Lu, Y., Luk, C. K., Maher, B., Pan, Y., Puhrsch, C., Reso, M., Saroufim, M., Siraichi, M. Y., Suk, H., Zhang, S., Suo, M., Tillet, P., Zhao, X., Wang, E., Zhou, K., Zou, R., Wang, X., Mathews, A., Wen, W., Chanan, G., Wu, P., and Chintala, S. Pytorch 2: Faster machine learning through dynamic python bytecode transformation and graph compilation. In *Proceedings of the 29th ACM International Conference on Architectural Support for Programming Languages and Operating Systems, Volume 2*, ASPLOS ’24, pp. 929–947, New York, NY, USA, 2024. URL <https://doi.org/10.1145/3620665.3640366>.

Asai, A., Wu, Z., Wang, Y., Sil, A., and Hajishirzi, H. Self-rag: Learning to retrieve, generate, and critique through self-reflection. In *The Twelfth International Conference on Learning Representations*, 2023.

Asai, A., He, J., Shao, R., Shi, W., Singh, A., Chang, J. C., Lo, K., Soldaini, L., Feldman, S., D’arcy, M., et al. Openscholar: Synthesizing scientific literature with retrieval-augmented lms. *arXiv preprint arXiv:2411.14199*, 2024a.

Asai, A., Wu, Z., Wang, Y., Sil, A., and Hajishirzi, H. Original implementation of self-rag: Learning to retrieve, generate and critique through self-reflection. <https://github.com/AkariAsai/self-rag>, 2024b.

Asai, A., Zhong, Z., Chen, D., Koh, P. W., Zettlemoyer, L., Hajishirzi, H., and Yih, W.-t. Reliable, adaptable, and attributable language models with retrieval. *arXiv preprint arXiv:2403.03187*, 2024c.

Berger, E. and Zorn, B. Ai software should be more like plain old software. <https://www.sigarch.org/ai-software-should-be-more-like-plain-old-software/>, 2024.

Borgeaud, S., Mensch, A., Hoffmann, J., Cai, T., Rutherford, E., Millican, K., Van Den Driessche, G. B., Lespiau, J.-B., Damoc, B., Clark, A., et al. Improving language models by retrieving from trillions of tokens. In *International conference on machine learning*, pp. 2206–2240. PMLR, 2022.

Chemmagate, B. Reducing rag pipeline latency for real-time voice conversations. <https://developer.vonage.com/en/blog/reducing-rag-pipeline-latency-for-real-time-voice-conversations>, 2024.

Chen, Q., Zhao, B., Wang, H., Li, M., Liu, C., Li, Z., Yang, M., and Wang, J. Spann: Highly-efficient billion-scale approximate nearest neighbor search. *arXiv preprint arXiv:2111.08566*, 2021.

Databricks. Rag (retrieval augmented generation) on databricks. <https://docs.databricks.com/en/generative-ai/retrieval-augmented-generation.html>, 2024.

Douze, M., Guzhva, A., Deng, C., Johnson, J., Szilvassy, G., Mazaré, P.-E., Lomeli, M., Hosseini, L., and Jégou, H. The faiss library. *arXiv preprint arXiv:2401.08281*, 2024.

Fan, W., Ding, Y., bo Ning, L., Wang, S., Li, H., Yin, D., Chua, T.-S., and Li, Q. A survey on rag meeting llms: Towards retrieval-augmented large language models. In *Knowledge Discovery and Data Mining*, 2024. URL <https://api.semanticscholar.org/CorpusID:269740933>.

Gao, L., Ma, X., Lin, J., and Callan, J. Precise zero-shot dense retrieval without relevance labels. In *Proceedings of the 61st Annual Meeting of the Association for Computational Linguistics (Volume 1: Long Papers)*, pp. 1762–1777, 2023a.

Gao, Y. Modular rag and rag flow: Part ii. <https://medium.com/@yufan1602/modular-rag-and-rag-flow-part-ii-77b62bf8a5d3>, 2024.

Gao, Y., Xiong, Y., Gao, X., Jia, K., Pan, J., Bi, Y., Dai, Y., Sun, J., and Wang, H. Retrieval-augmented generation for large language models: A survey. *arXiv preprint arXiv:2312.10997*, 2023b.

GM, A. and Dhar, G. How apollo 24—7 leverages medlm with rag to revolutionize healthcare. <https://cloud.google.com/blog/products/ai-machine-learning/how-apollo-247-leverages-medlm-with-rag-to-revolutionize-healthcare>, 2024.

Hardt, M. and Sun, Y. Test-time training on nearest neighbors for large language models. *arXiv preprint arXiv:2305.18466*, 2023.

Ilin, I. Advanced rag techniques: an illustrated overview. <https://pub.towardsai.net/advanced-rag-techniques-an-illustrated-overview-04d193d8fec6>, 2023.

Izacard, G., Caron, M., Hosseini, L., Riedel, S., Bojanowski, P., Joulin, A., and Grave, E. Unsupervised dense information retrieval with contrastive learning. *arXiv preprint arXiv:2112.09118*, 2021.

Izacard, G., Lewis, P., Lomeli, M., Hosseini, L., Petroni, F., Schick, T., Dwivedi-Yu, J., Joulin, A., Riedel, S., and Grave, E. Atlas: Few-shot learning with retrieval augmented language models. *Journal of Machine Learning Research*, 24(251):1–43, 2023.

Jagerman, R., Zhuang, H., Qin, Z., Wang, X., and Bender-sky, M. Query expansion by prompting large language models. *arXiv preprint arXiv:2305.03653*, 2023.

Jayaram Subramanya, S., Devvrit, F., Simhadri, H. V., Krishnawamy, R., and Kadekodi, R. Diskann: Fast accurate billion-point nearest neighbor search on a single node. *Advances in Neural Information Processing Systems*, 32, 2019.

Jiang, H., Wu, Q., Luo, X., Li, D., Lin, C.-Y., Yang, Y., and Qiu, L. Longllmlingua: Accelerating and enhancing llms in long context scenarios via prompt compression. *arXiv preprint arXiv:2310.06839*, 2023a.

Jiang, W., Li, S., Zhu, Y., de Fine Licht, J., He, Z., Shi, R., Renggli, C., Zhang, S., Rekatsinas, T., Hoefer, T., et al. Co-design hardware and algorithm for vector search. In *Proceedings of the International Conference for High Performance Computing, Networking, Storage and Analysis*, pp. 1–15, 2023b.

Jiang, W., Zhang, S., Han, B., Wang, J., Wang, B., and Kraska, T. Piperag: Fast retrieval-augmented generation via algorithm-system co-design. *arXiv preprint arXiv:2403.05676*, 2024.

Jiang, W., Subramanian, S., Graves, C., Alonso, G., Yazdanbakhsh, A., and Dadu, V. Rago: Systematic performance optimization for retrieval-augmented generation serving. *International Symposium on Computer Architecture*, 2025.

Jiang, Z., Xu, F. F., Gao, L., Sun, Z., Liu, Q., Dwivedi-Yu, J., Yang, Y., Callan, J., and Neubig, G. Active retrieval augmented generation. 2023c.

Jin, C., Zhang, Z., Jiang, X., Liu, F., Liu, X., Liu, X., and Jin, X. Ragcache: Efficient knowledge caching for retrieval-augmented generation. *arXiv preprint arXiv:2404.12457*, 2024a.

Jin, J., Zhu, Y., Yang, X., Zhang, C., and Dou, Z. Flashrag: A modular toolkit for efficient retrieval-augmented generation research. *arXiv preprint arXiv:2405.13576*, 2024b.

Johnson, J., Douze, M., and Jégou, H. Billion-scale similarity search with GPUs. *IEEE Transactions on Big Data*, 7 (3):535–547, 2019.

Joshi, M., Choi, E., Weld, D. S., and Zettlemoyer, L. Triviaqa: A large scale distantly supervised challenge dataset for reading comprehension. In *Proceedings of the 55th Annual Meeting of the Association for Computational Linguistics (Volume 1: Long Papers)*, pp. 1601–1611, 2017.

Karpukhin, V., Oguz, B., Min, S., Lewis, P., Wu, L., Edunov, S., Chen, D., and Yih, W.-t. Dense passage retrieval for open-domain question answering. In *Proceedings of the 2020 Conference on Empirical Methods in Natural Language Processing (EMNLP)*, 2020.

Khan, S., Singh, S., Simhadri, H. V., Vedurada, J., et al. Bang: Billion-scale approximate nearest neighbor search using a single gpu. *arXiv preprint arXiv:2401.11324*, 2024.

Khandelwal, U., Levy, O., Jurafsky, D., Zettlemoyer, L., and Lewis, M. Generalization through memorization: Nearest neighbor language models. In *International Conference on Learning Representations*, 2019.

Kim, J., Nam, J., Mo, S., Park, J., Lee, S.-W., Seo, M., Ha, J.-W., and Shin, J. Sure: Improving open-domain question answering of llms via summarized retrieval. In *The Twelfth International Conference on Learning Representations*, 2023.

Klang, E., Tessler, I., Apakama, D. U., Abbott, E., Glicksberg, B. S., Arnold, M., Moses, A., Sakhija, A., Soroush, A., Charney, A. W., et al. Assessing retrieval-augmented large language model performance in emergency department icd-10-cm coding compared to human coders. *medRxiv*, 2024.

Kwiatkowski, T., Palomaki, J., Redfield, O., Collins, M., Parikh, A., Alberti, C., Epstein, D., Polosukhin, I., Devlin, J., Lee, K., et al. Natural questions: a benchmark for question answering research. *Transactions of the Association for Computational Linguistics*, 7:453–466, 2019.

Kwon, W., Li, Z., Zhuang, S., Sheng, Y., Zheng, L., Yu, C. H., Gonzalez, J. E., Zhang, H., and Stoica, I. Efficient memory management for large language model serving with pagedattention. In *Proceedings of the ACM SIGOPS 29th Symposium on Operating Systems Principles*, 2023.

Lewis, P., Perez, E., Piktus, A., Petroni, F., Karpukhin, V., Goyal, N., Küttler, H., Lewis, M., Yih, W.-t., Rocktäschel, T., et al. Retrieval-augmented generation for knowledge-intensive nlp tasks. *Advances in Neural Information Processing Systems*, 33:9459–9474, 2020.

Liu, J. LlamaIndex. https://github.com/jerryliu/llama_index, 11 2022a.

Liu, J. MultiStep Query Engine LlamaIndex. https://developers.llamaindex.ai/python/examples/workflow/multi_step_query_engine/, 11 2022b.

Liu, J. Sub Question Query Engine LlamaIndex. https://developers.llamaindex.ai/python/examples/query_engine/sub_question_query_engine/, 11 2022c.

Lu, S., Wang, H., Rong, Y., Chen, Z., and Tang, Y. Turborag: Accelerating retrieval-augmented generation with pre-computed kv caches for chunked text. *arXiv preprint arXiv:2410.07590*, 2024.

Ma, X., Gong, Y., He, P., Duan, N., et al. Query rewriting in retrieval-augmented large language models. In *The 2023 Conference on Empirical Methods in Natural Language Processing*, 2023.

Malec, M. Rag in financial services: Use-cases, impact, & solutions. <https://hatchworks.com/blog/gen-ai/rag-for-financial-services/>, 2024.

Mallen, A. T., Asai, A., Zhong, V., Das, R., Khashabi, D., and Hajishirzi, H. When not to trust language models: Investigating effectiveness of parametric and non-parametric memories. In *The 61st Annual Meeting Of The Association For Computational Linguistics*, 2023.

Min, S., Gururangan, S., Wallace, E., Shi, W., Hajishirzi, H., Smith, N. A., and Zettlemoyer, L. Silo language models: Isolating legal risk in a nonparametric datastore. In *The Twelfth International Conference on Learning Representations*, 2023.

MyScale. 4 key benefits of rag algorithmic trading in financial markets. <https://myscale.com/blog/benefits-rag-algorithmic-trading-financial-markets/>, 2024.

Norouzi, M. and Fleet, D. J. Cartesian k-means. In *Proceedings of the IEEE Conference on computer Vision and Pattern Recognition*, pp. 3017–3024, 2013.

OpenAI. Gpt-3.5 turbo. <https://platform.openai.com/docs/models/gpt-3-5-turbo>.

Peng, W., Li, G., Jiang, Y., Wang, Z., Ou, D., Zeng, X., Tongxu, and Chen, E. Large language model based long-tail query rewriting in taobao search. *Companion Proceedings of the ACM on Web Conference 2024*, 2023. URL <https://api.semanticscholar.org/CorpusID:265042961>.

Peng, W., Li, G., Jiang, Y., Wang, Z., Ou, D., Zeng, X., Xu, D., Xu, T., and Chen, E. Large language model based long-tail query rewriting in taobao search. In *Companion Proceedings of the ACM on Web Conference 2024*, 2024.

Press, O., Zhang, M., Min, S., Schmidt, L., Smith, N. A., and Lewis, M. Measuring and narrowing the compositionality gap in language models. In *Findings of the Association for Computational Linguistics: EMNLP 2023*, pp. 5687–5711, 2023.

Quinn, D., Nouri, M., Patel, N., Salihu, J., Salemi, A., Lee, S., Zamani, H., and Alian, M. Accelerating retrieval-augmented generation. In *Proceedings of the 30th ACM International Conference on Architectural Support for Programming Languages and Operating Systems, Volume 1*, ASPLOS '25, pp. 15–32, New York, NY, USA, 2025. Association for Computing Machinery. ISBN 9798400706981. doi: 10.1145/3669940.3707264. URL <https://doi.org/10.1145/3669940.3707264>.

Ram, O., Levine, Y., Dalmedigos, I., Muhlgay, D., Shashua, A., Leyton-Brown, K., and Shoham, Y. In-context retrieval-augmented language models. *Transactions of the Association for Computational Linguistics*, 11:1316–1331, 2023.

Rapidsai. Rapidsai/raft: Raft contains fundamental widely-used algorithms and primitives for data science, graph and machine learning. <https://github.com/rapidsai/raft>, 2022.

Sella, A. Flash is driving scale in rag-based llms. In *Proceedings of the Flash Memory Summit (FMS)*, August 2024. URL https://files.futurememorystorage.com/proceedings/2024/20240807_AIML-203-1_Sella.pdf. Session AIML-203-1.

Shao, R., He, J., Asai, A., Shi, W., Dettmers, T., Min, S., Zettlemoyer, L., and Koh, P. W. Scaling retrieval-based language models with a trillion-token datastore. In *The Thirty-eighth Annual Conference on Neural Information Processing Systems*.

Shao, Z., Gong, Y., Shen, Y., Huang, M., Duan, N., and Chen, W. Enhancing retrieval-augmented large language models with iterative retrieval-generation synergy. In *Findings of the Association for Computational Linguistics: EMNLP 2023*, pp. 9248–9274, 2023.

Shen, M., Umar, M., Maeng, K., Suh, G. E., and Gupta, U. Hermes: Algorithm-system co-design for efficient retrieval-augmented generation at-scale. *International Symposium on Computer Architecture*, 2025.

Sivic, J. and Zisserman, A. Video google: A text retrieval approach to object matching in videos. In *ICCV*, pp. 1470–1477. IEEE Computer Society, 2003.

Stewart, D. and Linsdell, J. Say hello to precision: How rerankers and embeddings boost search. <https://cohere.com/blog/say-hello-to-precision-how-rerankers-and-embeddings-boost-search>, 2024.

The ZeroMQ authors. ZeroMQ. <https://zeromq.org/>, 2025.

Touvron, H., Martin, L., Stone, K., Albert, P., Almahairi, A., Babaei, Y., Bashlykov, N., Batra, S., Bhargava, P., Bhosale, S., et al. Llama 2: Open foundation and fine-tuned chat models. *arXiv preprint arXiv:2307.09288*, 2023.

Tung, K. Enhancing user experience by overcoming latency in the ion iq chatbot. <https://www.ontinue.com/resource/enhancing-user-experience-by-overcoming-latency-in-the-ion-iq-chatbot/>, 2024.

Wang, L., Ma, C., Feng, X., Zhang, Z., Yang, H., Zhang, J., Chen, Z., Tang, J., Chen, X., Lin, Y., et al. A survey on large language model based autonomous agents. *Frontiers of Computer Science*, 18(6):186345, 2024.

Wei, K. Advanced rag with azure ai search and llamaindex. <https://techcommunity.microsoft.com/t5/ai-azure-ai-services-blog/advanced-rag-with-azure-ai-search-and-llamaindex/ba-p/4115007>, 2024.

Xie, Z., Kang, H., Sheng, Y., Krishna, T., Fatahalian, K., and Kozyrakis, C. Ai metropolis: Scaling large language model-based multi-agent simulation with out-of-order execution. *arXiv preprint arXiv:2411.03519*, 2024.

Yang, Z., Qi, P., Zhang, S., Bengio, Y., Cohen, W. W., Salakhutdinov, R., and Manning, C. D. HotpotQA: A dataset for diverse, explainable multi-hop question answering. In *Conference on Empirical Methods in Natural Language Processing (EMNLP)*, 2018.

Yao, J., Li, H., Liu, Y., Ray, S., Cheng, Y., Zhang, Q., Du, K., Lu, S., and Jiang, J. Cacheblend: Fast large language model serving for rag with cached knowledge fusion, 2024. URL <https://arxiv.org/abs/2405.16444>.

Ye, F., Fang, M., Li, S., and Yilmaz, E. Enhancing conversational search: Large language model-aided informative query rewriting. In *The 2023 Conference on Empirical Methods in Natural Language Processing*, 2023.

Zaharia, M., Khattab, O., Chen, L., Davis, J. Q., Miller, H., Potts, C., Zou, J., Carbin, M., Frankle, J., Rao, N., and Ghodsi, A. The shift from models to compound ai systems. <https://bair.berkeley.edu/blog/2024/02/18/compound-ai-systems/>, 2024.

Zhang, Z., Liu, F., Huang, G., Liu, X., and Jin, X. Fast vector query processing for large datasets beyond GPU memory with reordered pipelining. In *21st USENIX Symposium on Networked Systems Design and Implementation (NSDI 24)*, pp. 23–40, 2024a.

Zhang, Z., Zhu, A., Yang, L., Xu, Y., Li, L., Phothilimthana, P. M., and Jia, Z. Accelerating retrieval-augmented language model serving with speculation. *arXiv preprint arXiv:2401.14021*, 2024b.

Zheng, H. S., Mishra, S., Chen, X., Cheng, H.-T., Chi, E. H., Le, Q. V., and Zhou, D. Take a step back: Evoking reasoning via abstraction in large language models. *arXiv preprint arXiv:2310.06117*, 2023.

Zheng, L., Yin, L., Xie, Z., Sun, C., Huang, J., Yu, C. H., Cao, S., Kozyrakis, C., Stoica, I., Gonzalez, J. E., Barrett, C., and Sheng, Y. Sglang: Efficient execution of structured language model programs, 2024. URL <https://arxiv.org/abs/2312.07104>.

Zhou, D., Schärli, N., Hou, L., Wei, J., Scales, N., Wang, X., Schuurmans, D., Cui, C., Bousquet, O., Le, Q. V., et al. Least-to-most prompting enables complex reasoning in large language models. In *The Eleventh International Conference on Learning Representations*, 2022.

Zhuang, S., Liu, B., Koopman, B., and Zucco, G. Open-source large language models are strong zero-shot query likelihood models for document ranking. In *Findings of the Association for Computational Linguistics: EMNLP 2023*, pp. 8807–8817, 2023.

Zilliz. How to select index parameters for ivf index. <https://zilliz.com/blog/select-index-parameters-ivf-index>, 2020.

A BACKGROUND: INVERTED FILE INDEX (IVF) FOR VECTOR SEARCH

The *vector index* is a crucial component of RAG applications that retrieves similar items from large datasets of high-dimensional vectors. Given the query vector $x \in \mathbb{R}^D$ and vector database $Y = \{y_0, \dots, y_{N-1}\} \subset \mathbb{R}^D$, which comprises N vectors, the vector index aims to find the k nearest neighbors of x from the database:

$$k\text{-argmin}_{i=0:N} d(x, y_i),$$

where D is the dimensionality of the vector determined by the embedding model, and d denotes the distance function, which is typically the L2-norm or inner product (Johnson et al., 2019).

To improve search efficiency, the inverted file index (IVF) algorithm is widely used for large-scale vector databases due to its simplicity and effectiveness. IVF partitions the data store into *clusters* and restricts searches to the most relevant clusters, reducing the computational cost. To obtain the cluster assignment of each stored vector, it performs clustering algorithm such as k -means (Norouzi & Fleet, 2013) and partitions the database into N_c clusters:

$$\{C_1, C_2, \dots, C_{N_c}\} = k\text{-means}(Y, N_c),$$

where C_j is the set of vectors assigned to the j -th cluster, and the cluster centroids $\{c_1, c_2, \dots, c_{N_c}\}$ are obtained by taking the mean of each vectors in $\{C_1, C_2, \dots, C_{N_c}\}$. Then, each database vector $y_i \in Y$ is assigned to the nearest cluster center:

$$\text{Cluster}(y_i) = \text{argmin}_{j=1:N_c} d(y_i, c_j).$$

With the trained centroids and cluster assignment, we can perform a more efficient index search. There are two steps involved in the IVF index searching. First, it will identify the nearest L cluster centroids of a query vector x :

$$\{c_{j_1}, c_{j_2}, \dots, c_{j_L}\} = L\text{-argmin}_{j=1:C} d(x, c_j).$$

This step is also referred to as the coarse-grained search in IVF, as it identifies candidates at the cluster level. Second, the fine-grained search is performed in the L nearest clusters and identify k closest vectors of x :

$$k\text{-argmin}_{y_i \in \cup_{l=1}^L C_{j_l}} d(x, y_i).$$

which involves sorting. In this way, IVF reduces search space and accelerates the retrieval process. Here, the hyper-parameter L from the first step is also referred as `nprobe` (Douze et al., 2024). When `nprobe` is larger, the IVF retrieval will be more accurate as it search more clusters. However, the retrieve latency is longer as more computation and data are needed.

B FINDING PREFETCHING AMOUNT

A key challenge in TELERAG is to balance the benefit of reducing retrieval latency by prefetching data against the overhead of CPU-GPU transfers. Prefetching more clusters reduces the subsequent retrieval time but can also extend the transfer phase; if it extends beyond the LLM generation window, we lose the advantage of overlap and potentially introduce additional delay. Still, additional delays in data transfer may be worthwhile if they substantially reduce retrieval latency. To guide the choice of the optimal amount of data to prefetch, we develop a mathematical model based on profile information.

Mathematical model. Here, we denote b_p as the number of bytes to prefetch and B as the CPU-GPU bandwidth. The optimal amount of data to prefetch is denoted as b_p^* . To start, we let t_1 represent the combined time of prefetching and pre-retrieval LLM generation, and t_2 represents the retrieval time. We have: $t_1 = \max(t_{\text{LLM}}, t_p)$ and $t_2 = \max(t_c, t_g)$, where t_{LLM} is the time for LLM generation, t_p is prefetching time, t_c is the CPU retrieval time, and t_g is the GPU retrieval time. The objective is to minimize $t_1 + t_2$.

Since prefetching time t_p is proportional to b_p , we express t_1 as a piecewise function:

$$t_1 = \begin{cases} t_{\text{LLM}}, & \text{if } b_p \leq B \cdot t_{\text{LLM}}, \\ \frac{b_p}{B}, & \text{if } b_p > B \cdot t_{\text{LLM}}, \end{cases} \quad (1)$$

From Eq. 1, if we prefetch fewer bytes than can be transferred during LLM generation, t_1 is effectively just t_{LLM} because the transfer overlaps completely with LLM execution.

As shown in the analysis section, GPU retrieval (t_g) is generally much faster than CPU retrieval (t_c). Thus, we assume $t_c \gg t_g$. As CPU has a limited parallelism, t_c usually grows proportionally with the number of clusters to be processed (Jiang et al., 2023b):

$$t_2 = t_c = r_{\text{miss}} \times n_{\text{probe}} \times t_{\text{cc}}, \quad (2)$$

where r_{miss} is the miss rate (percentage of IVF clusters are not caught on GPU), n_{probe} is the total number of clusters to search, and t_{cc} is the CPU time to search a single cluster. Increasing b_p can only decrease or maintain the current miss rate, i.e., $\frac{dr_{\text{miss}}}{db_p} \leq 0$. Moreover, because clusters are prefetched in order of descending likelihood, we assume r_{miss} is either linear or a concave up function¹ of b_p , i.e., $\frac{d^2 r_{\text{miss}}}{db_p^2} \geq 0$.

We now examine two cases:

¹An upward U-shaped function whose second derivative is positive.

- **Case 1:** $b_p^* \leq B \cdot t_{\text{LLM}}$. Here, $t_1 = t_{\text{LLM}}$ is constant because prefetching is fully overlapped with LLM generation. Since increasing b_p in this regime will not increase t_1 and cannot worsen the miss rate, pushing b_p to the boundary $B \cdot t_{\text{LLM}}$ minimizes $t_1 + t_2$. Hence,

$$b_p^* = B \cdot t_{\text{LLM}}. \quad (3)$$

- **Case 2:** $b_p^* > B \cdot t_{\text{LLM}}$. In this region, t_1 grows linearly with b_p , and we have: $\frac{d^2}{db_p^2}(t_1 + t_2) = \frac{d^2 r_{\text{miss}}}{db_p^2} \cdot n_{\text{probe}} \cdot t_{\text{cc}} \geq 0$. Therefore, $t_1 + t_2$ is concave up, allowing at most one minimum. At the minimum point, we have:

$$\frac{d}{db_p}(t_1 + t_2) = 0 \implies \frac{1}{B} + \frac{dr_{\text{miss}}}{db_p} \cdot n_{\text{probe}} \cdot t_{\text{cc}} = 0. \quad (4)$$

From this, we obtain:

$$b_p^* = B \times n_{\text{probe}} \times t_{\text{cc}} \times \Delta r_{\text{miss}}, \quad (5)$$

where Δr_{miss} is the decrement of the miss rate for this round. If b_p^* is indeed larger than $B \cdot t_{\text{LLM}}$, it becomes the global minimum; otherwise, the solution reverts to Case 1.

In summary, our analysis shows that the optimal prefetch amount b_p^* can only lie at one of two points: (1) Prefetch until LLM generation completes (i.e. $b_p = B \cdot t_{\text{LLM}}$). (2) A point determined by Eq. 5. However, under typical CPU-GPU bandwidth (e.g., 64 GB/s on PCIe 5), the time spent loading additional clusters often outweighs any retrieval latency reduction from lowering r_{miss} . Consequently, the second scenario in Eq. 5 becomes nearly infeasible in practice. Therefore, on current hardware, *prefetching exactly until LLM execution ends* is generally the most effective choice.

C IMPLEMENTATION DETAILS

TELERAG is implemented in Python and also leverages PyTorch’s (Ansel et al., 2024) operator ecosystem for efficient computation. The datastore index is initially constructed using FAISS (Douze et al., 2024), and its data structures, such as IVF centroids and cluster data, are converted to PyTorch tensors.

At runtime, cluster data is loaded into a contiguous pinned memory region on the CPU, enabling non-blocking memory copies to the GPU. A fixed-size contiguous buffer on the GPU is allocated based on the user’s configuration or GPU memory capacity during runtime.

We use separate processes for the schedulers and services in TELERAG to avoid bottlenecks in Python global interpreter lock. For the communication between the scheduler and the services, we also leverages the ZeroMQ (The ZeroMQ

authors, 2025) as the communication framework. The message is encoded and decoded with Pickle in Python. For the LLM service, we use SGLang (Zheng et al., 2024) as the LLM backend. For the retrieval service, to implement the index search with GPU-CPU cooperation, on GPU, we use a single matrix-vector multiplication that computes distances for all prefetched vectors; on CPU, we utilize multithreading in Python to parallelize similarity searches across clusters. We then move the distances computed from CPU to GPU, merge with results on GPU and perform global sorting on GPU.

To monitor the hotness of cached clusters better, we use a **decay-based** approach to track the hotness of cached clusters. Every cached cluster has a hotness value. Upon fetching to the GPU, the cluster is essentially cached and will be assigned with a initial value $h_0 = h_{\text{init}}$. Then, when a new round of hotness update starts, the hotness will be divided with a decay factor d , and if the cluster is used in the previous round, an hotness update value h_{inc} will be added the hotness. Therefore, the transition of hotness from the round r to round $r + 1$ can be given as:

$$h_{r+1} = \begin{cases} h_r/d, & \text{if not used in round } r, \\ h_r/d + h_{\text{inc}}, & \text{if used in round } r. \end{cases} \quad (6)$$

In this way, the process can be parallelized easily on GPU, minimize the overhead of hotness tracking in terms of both the time and computation. We also set a cache fraction, which means if the cache exceeds the fraction, we need to evict some clusters. The cache fraction is set to 0.5 by default. To make evaluation result stable and reproducible, we do cache eviction for the excessive clusters and consolidate the GPU memory after serving each batch. This makes sure that we will not over-evaluate the performance of the caching system.

Both schedulers use greedy search to minimize overhead. The prefetching scheduler groups similar queries into mini-batches, and feeds them into the cache-aware scheduler to assign mini-batches to GPUs. The cache-aware scheduler will get the number of overlapped clusters on each GPU for each mini-batch, and assign the mini-batch to the GPU with the most overlapped clusters.

D DETAILED INDEX CONFIGURATIONS

Table 4 shows the detailed configurations of our retrieval index used in the evaluation.

Specification	Value
Dataset	wiki_dpr (Karpukhin et al., 2020)
Dataset size	2.1 billion tokens
# of chunks	21 million
# of IVF cluster	4096
Embed model	Contriever (Izacard et al., 2021)
Embed dimension	768
Index type	FLAT ²
Distance metric	Inner Product
Index size	61 GB

Table 4. Detailed configurations of our retrieval index.

²Original embedding without compression for the best retrieval precision.